INFLUENCE OF WINGLETS ON THE TIP VORTEX OF LOW PRESSURE AXIAL FANS

Daniel KESSLER[1], Jens FRIEDRICHS[1], Frieder LÖRCHER[2]

[1] *TU Braunschweig, Institute of Jet Propulsion and Turbomachinery, Hermann-Blenk-Straße 37, 38108 Braunschweig, Germany*

[2]*ZIEHL-ABEGG SE, Heinz-Ziehl-Straße, 74653 Künzelsau, Germany*

SUMMARY

A primary goal of the ventilation, air conditioning industry, and the automotive industry is the reduction of noise emission to fulfill regulations and customer demands. The tip vortex, one of the sources for a high sound power level, can be influenced by the blade sweep and design of the blade tip geometry. This paper aims to investigate three different blade tip geometries or winglets. By using basic designs, the fundamental influence on the behavior of the tip vortex and the noise generation is shown. Aerodynamic (including performance curve and wall pressure measurements) and aeroacoustic studies are carried out. The results of the different blade tip geometries are compared to a baseline fan with available data.

INTRODUCTION

Fans serve a wide range of applications with respect to aerodynamic and geometric requirements. They can provide large volume flow rates and low pressure rise coefficients. For newly designed fans next to aerodynamic and geometric specifications, acoustic limits and minimum efficiency requirements have to be taken into account [1].

The noise emission can be separated into four mechanisms [2]: steady-state (in the rotating system), blade forces like lift and drag, flow displacement due to the blade thickness, and unsteady blade forces. Unsteady blade forces can be further divided into unsteady inflow, secondary flow phenomena, vortex separation, turbulent boundary layer, and other effects [3]. Considering its spectral content the noise emission can be divided into discrete frequencies (blade passing frequency, harmonics) and broadband noise (separations, turbulent boundary layer).

One of these sources is the gap vortex, which forms in the gap between blade and casing due to the pressure difference between the suction and pressure side. Marcinowski (1953) [4] detected the vortex in the frequency spectrum as a broadband phenomenon. As the gap width increases, the

spectral width grows and shifts toward smaller frequencies. According to Khorrami *et al.* [5], the noise emission is based on two mechanisms: the self-noise and the interaction of the vortex with other blades. For single-row fans, a downstream stator is of no concern. But the interaction with the subsequential neighbor blade is. Similar results are shown by Fukano and Yang, who measured the velocity distribution and fluctuations of the blade tip vortex at different operating points using hot-wire measurements. They were able to show that the blade tip noise is caused, on the one hand, by the interaction of the vortex with the suction-side of the corresponding rotor blade, and on the other hand, with the pressure side of the following blade [6]. The pressure difference of the blade defines the strength of the vortex, while the shape depends on the shape of the tip gap. The initial idea is to reduce the gap. Longhouse [7] showed that a narrow gap reduces the emitted A-weighted sound level by up to 15 dB(A). Second, active methods and passive shaping options are possible to influence the flow in the gap in a positive way. For example, installing a co-rotating ring around the blade tip can reduce the sound level by up to 12 dB(A) [7].

A smaller gap is better, according to all research results [4-8]. However, the manufacturing effort is significantly higher. Alternatively, the shape of the blade can be adapted at the tip to influence the flow. Past studies investigated several different blade tip geometries. While Zhang *et al.* [9] changed the blade tip in the radial direction; Corsini *et al.* [10] and Nashimoto *et al.* [11] showed acoustic improvements with a thickened blade tip in axial fans. Zhang *et al.* [12] used a similar design method for a diagonal fan. They showed experimentally and numerically minor influences on the aerodynamic performance while achieving good acoustic results. In their papers [10-12], they refer to the thickened blade tip as winglets.

Since winglets show a positive effect, further investigations are made in this paper. Therefore, generic and geometrically simple winglets are designed and tested. The aerodynamic and acoustic performance is discussed and compared to a baseline fan without winglets. As two effects of noise emission occur regarding the tip vortex (self-blade-interaction and interaction with the neighbor blade), the question is, which effect is more important and how they are affected by the winglet.

EXPERIMENTAL SETUP

Test facility

All measurements, except for the acoustic tests, were performed at a test rig at the University of Braunschweig. Figure 1 shows the test rig. The test rig is a so-called inlet-side test chamber with a free inlet and a free outlet stage installation [13]. Using a standard nozzle according to [14] at the test rig inlet, the volume flow rate is measured. Further downstream, the volume flow is assumed constant. Therefore, flow velocity and dynamic pressure can be calculated as functions of the cross-sectional area. Flow straighteners and screens upstream of the fan ensure uniform flow conditions for the test object.

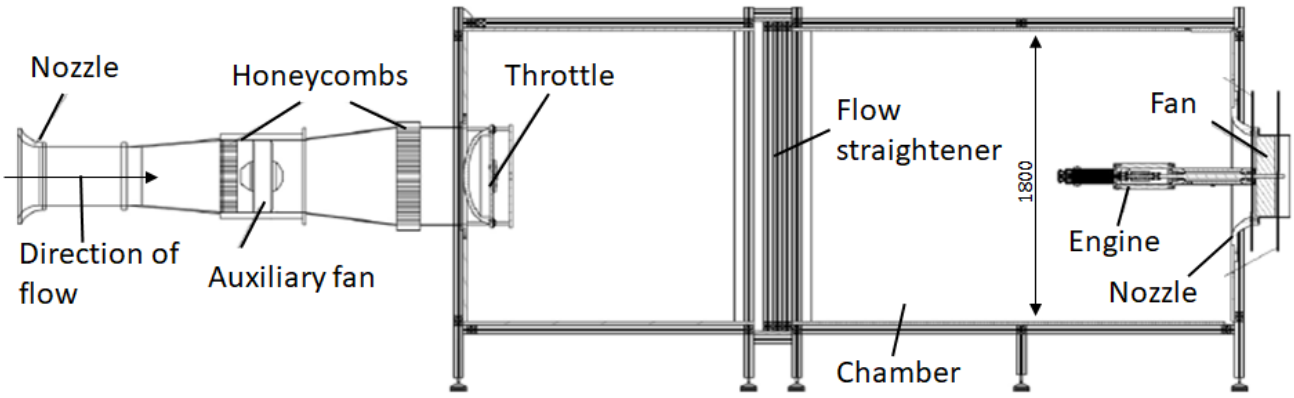

Figure 1: Low-pressure axial fan test rig at Technical University of Braunschweig

The flow coefficient φ can be adjusted by a throttle in order to investigate different operating points. An additional auxiliary fan is used to compensate for losses in the test rig. Thereby higher flow rates can be achieved.

Inside the test rig the total-to-static pressure difference between the test chamber upstream of the axial fan and ambient environment is measured. The measured Mach number in the fan is below 0.2; therefore, the flow can be considered incompressible. A full-length nozzle upstream of the fan with D_{nozzle} = 503 mm was used for all measurements. A cylindrical tube with a constant diameter extends the nozzle to measure the wall pressure close to the tip (see Figure 2 bottom right). The motor and measurements for torque and rotational speed are installed upstream.

Fan

The baseline fan design (Fan 2.2) is described by Lindemann *et al.* [15]. The baseline blade has aerodynamic airfoil sections designed under the specification of pressure rise and flow coefficient and empirical curves for the meridional velocity. Furthermore, sweep in a pure axial direction without shifting the blade in a circumferential direction (dihedral) was added. For this, all airfoil sections of an unswept blade are shifted in the positive (back sweep) or negative (forward sweep) direction along the airfoil chord direction. The arc angle δ is defined using the form parameters A = 0.72 and B = 2, ν = 0.3 and δ_{max} = 30° as:

$$\delta/\delta_{max} = e^{A \cdot R^B} - e^{A \cdot \nu^B} \quad (1)$$

with $R = r/r_{max}$ being the non-dimensional radius. This method of introducing sweep can lead to local discontinuities, especially in the curvature of the leading edge. Therefore, the profile is smoothed with a digital 1D filter. The reduction of the profile load and thus of the work transfer associated with the sweeping effect has to be compensated. In aircraft wing theory, a similar reduction of lift and lift slope is well known. The respective profile sections are corrected by a cosϕ approach [16]. The result is a blade with increasing sweep towards larger radii, especially in the outer region for R > 66 %.

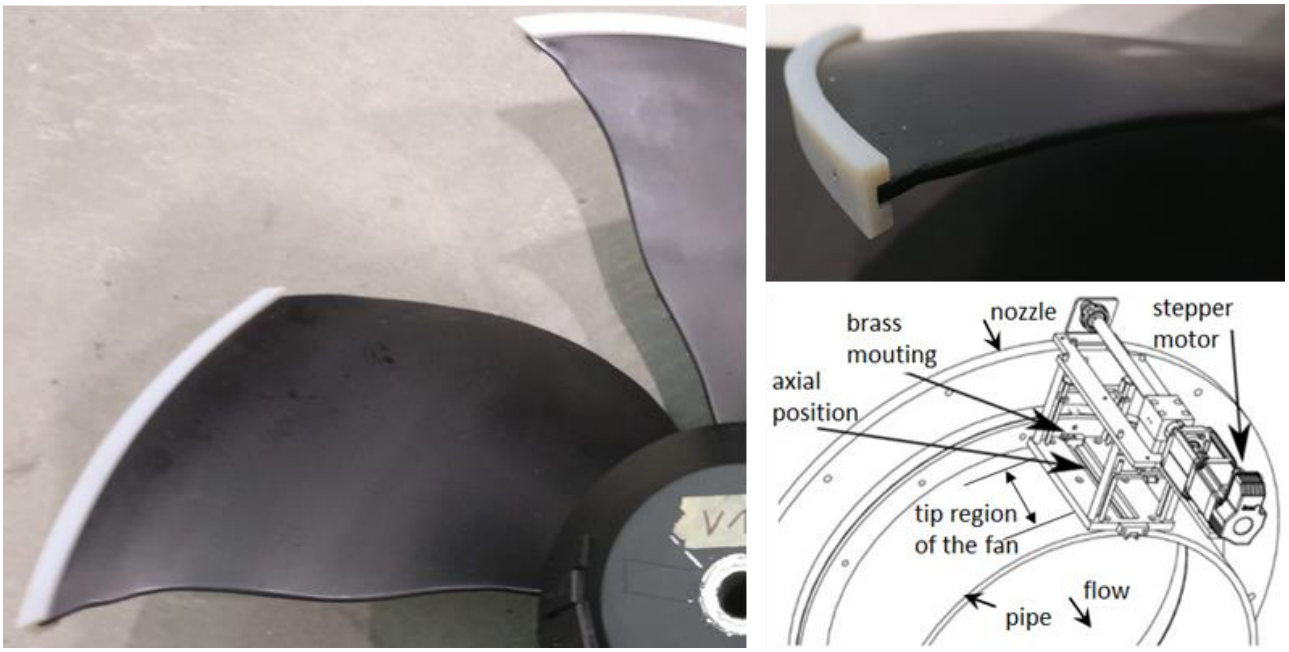

Figure 2: Fan V1 with "both-sides" winglets (left), close-up of blade tip seen from leading edge (top right), schematic structure of wall pressure measurements (bottom right)

Further tests with this fan were carried out by Skorpel *et al.* (Fan V1) using a variation with higher blade thickness [17]. As a baseline fan, the thickened blade V1 is used in this paper, which is shown

in Figure 2 on the left. V1 is a low-pressure axial fan with five blades. The blades have a constant thickness of 4 mm and a maximum chord length of l = 190 mm. The non-dimensional tip clearance in respect to the chord length s/l is about 1.6 percent. Further stage parameters are summarized in Tab. 1. The Reynolds number Re = $4.5 \cdot 10^5$ is calculated with the chord length and tip speed.

Theoretically, a variety of parameters of the winglet design can be investigated. Still, a generic winglet design was chosen. Thereby basic principles have been investigated, and the results can be transferred more easily to different fan designs.

The winglets are manufactured using rapid prototyping. For simple assembly and easy adjustments, the winglets are not only thickening the blade in the tip region but replacing a part of the blade tip as well. Therefore, the blade diameter of the baseline fan has been reduced to 492 mm. A part of the winglet replaces the outer blade and restores the original geometry. In total, four different winglet geometries have been investigated. The "neutral" winglet restores the original V1 geometry. This gives a comparison of test results using the original baseline fan and the fan with the restored geometry using prototyped blade tips. The “pressure-side” and “suction-side” winglets thicken the blade by 4.6 mm in the radially outer 4 mm of the blade in the corresponding direction. The fourth winglet combines the pressure- and suction-side winglet and is therefore called “both-sides”. Figure 2 shows the installed “both-sides” winglet in the top right corner.

Table 1: Stage design parameters

Design point objective	**Formula**	**Value**	**Unit**
Flow coefficient	$\varphi = \frac{4 \cdot q_V}{\pi^2 (D_t^2 - D_h^2) D_t n}$	0.23	1
Pressure rise coefficient	$\psi_{ts} = \frac{2 \cdot \Delta p_{ts}}{\rho (\pi D_t n)^2}$	0.19	1
Efficiency	$\eta_{ts} = \frac{q_V \cdot \Delta p_{ts}}{P_{mech}}$	0.53	1
Hub to tip ratio	$\nu = \frac{D_h}{D_t}$	0.30	1
Rotational speed	n	22.5	1/s

Measurements

Performance measurements

The definitions of the main parameters for characteristic measurements (volume flow rate, pressure rise coefficient, and efficiency) are shown in Table 1. Due to the free discharge of the flow into the pressure side environment, the dynamic pressure downstream of the fan is neglected for the calculation of the pressure rise. The pressure rise coefficient and the efficiency are therefore calculated as total-to-static. According to [18] and [19], the static pressure downstream of the fan can be assumed to be ambient pressure. For a characteristic curve, around 25 operating points are measured. Each operating point is the arithmetic mean calculated over 100 measurements. Thereby fluctuations in the flow are canceled out.

Acoustic measurements

All acoustic measurements were performed at the combined performance and noise measurement test rig of ZIEHL-ABEGG SE (see [20]) according to [21]. For the measurement, the fan is installed in a wall in between two enclosed and anechoic rooms. The rooms are connected by an air circuit which minimizes external noise and feedback effects. The noise emission is measured using

microphone arrays mounted on the suction and pressure side in the far-field of the fan. The difference between suction and pressure side measurements is low. Therefore only results of the pressure side are shown, including A-weighted sound power levels and one-third octave bands.

Wall pressure measurements

Figure 2 (bottom right corner) shows the basic structure of the wall pressure measurements. A high-resolution pressure sensor (Kulite XCS 190(M)) is embedded perpendicularly in the tube wall to investigate the tip vortex. The pressure recorded at 1024 positions per revolution is averaged over 64 revolutions at 90 axial positions at an axial distance of 1.5 mm each. The axial position is adjusted using a traversing unit with a stepper motor. An incremental rotary encoder is installed in the driveshaft to synchronize the measurements in the circumferential direction. The encoder gives a reference signal and 1024 clock signals per revolution. Thus, fluctuations in speed do not affect the measurement results. 1024 measurements per revolution lead to an angle resolution of 0.35°. The measurement signal from the sensor is amplified and recorded using a transient recorder. The measured voltage signal of the pressure sensor is converted into a pressure signal, using the calibration of the sensor after the measurement. The pressure coefficient is calculated with respect to the tip velocity at the casing:

$$c_p = {2 \cdot \bar{p}_c(x, U)} \Big/ {\rho \cdot u_t^2} \qquad (2)$$

RESULTS

Performance curves

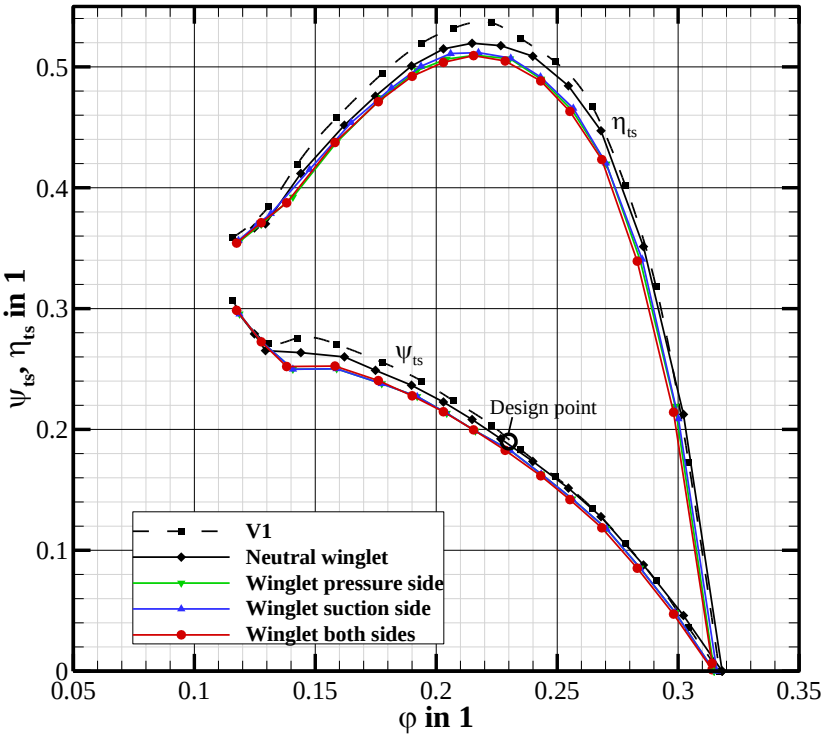

Figure 3: Characteristic and efficiency of all winglet configurations and V1

Figure 3 shows the performance curves of all winglet configurations. The performance of V1 and "neutral" winglet differ from each other. The "neutral" winglet has a reduced efficiency starting from about φ = 0.27 towards partial load. Furthermore, the pressure rise is lower beginning at the design point. It is assumed that the tip gap width is responsible for this effect. The cast geometry of the V1 has a varying tip gap width between 2.5 and 3.0 mm, with a mean value of 2.7 mm. The

blades with installed winglets have a constant gap width of 3.0 mm. The smaller gap leads to a higher pressure rise and thus also to an increased efficiency [22]. Consequently, the reference of the "pressure-", "suction-" and "both-sides" winglets is the "neutral" winglet in order to neglect the influence of the tip gap width when evaluating the winglet effect.

Along the entire range, the characteristic curves of the winglet configurations ("pressure-", "suction-", "both-sides") are similar regarding pressure rise and efficiency. Compared to the "neutral" winglet, they have a reduced pressure rise and efficiency. At the design point, the pressure rise is 2 percent lower, while the efficiency is decreased by 1 percentage point. This difference decreases for higher flow rates. The winglets have a neglectable impact on the integral values of the characteristic curve. A more complex-shaped winglet may reduce the disadvantage.

Acoustic measurements

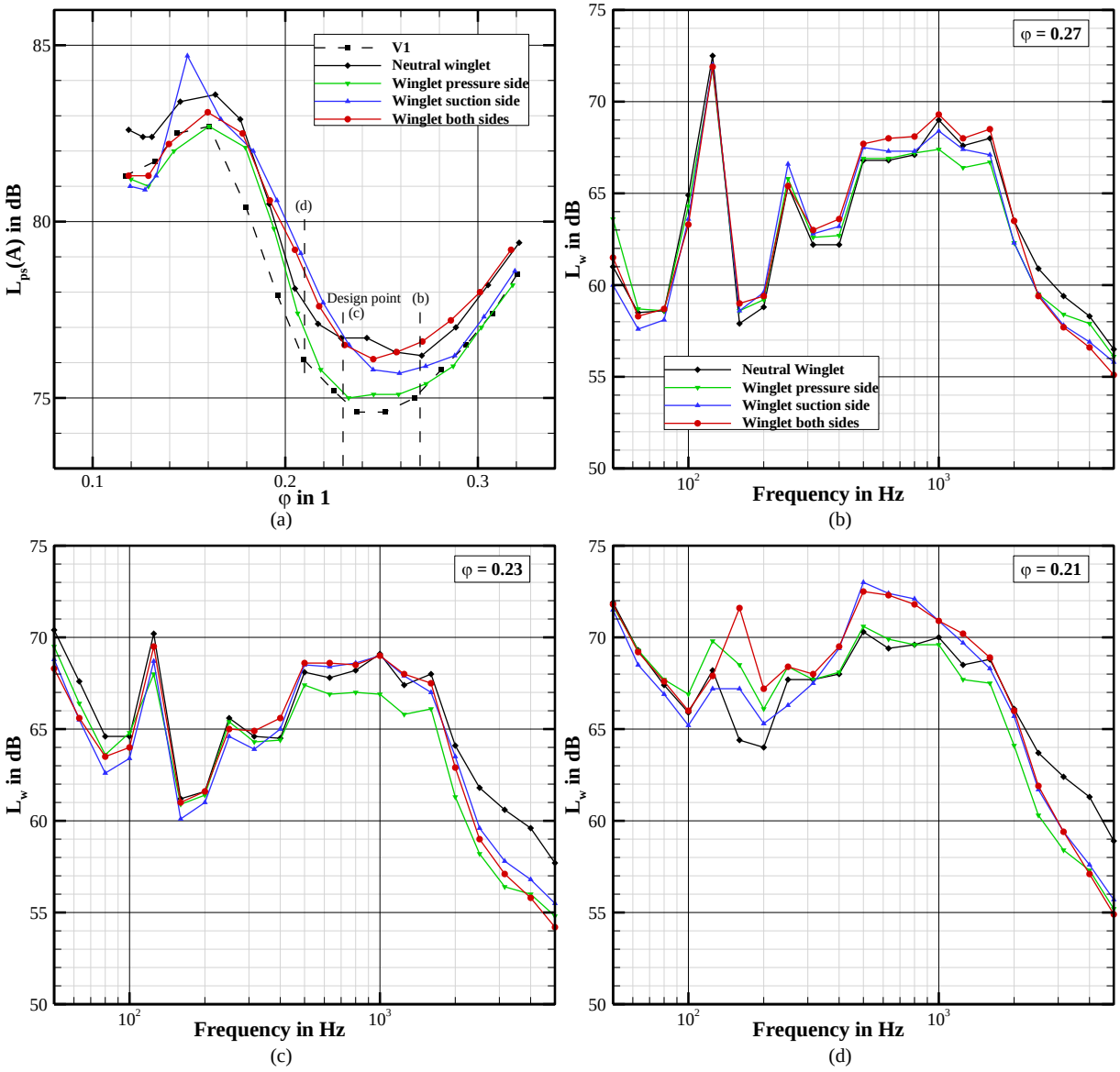

Figure 4: Pressure side measured A-Weighted sound power level of all winglet configurations and V1 (a), One-third-octave band of all winglet configurations for φ = 0.27 (b); φ = 0.23 (c); φ = 0.21(d)

Compared to the "neutral" winglet, a reduction in the noise emission for the "suction-" and "pressure-" side winglets can be seen in the A-weighted sound power level (see Figure 4 (a)). The positive effect occurs at overload (high φ) up to the design point. At partial load (low φ), this advantage over the "neutral" winglet is lost for the "suction-side" winglet but continues for the

“pressure-side” winglet at lower volume flow rates. At the design point, the “pressure-side” winglet has a lower sound power level of approximately 1.5 to 2 dB compared to the “neutral” winglet and can compete with V1. This reduction is quite significant compared to the small dimensions of the winglets. Compared to the reference V1, all winglet variants have a higher sound power level over a wide range of the characteristic curve. Only the “pressure-side” winglet can compete with the acoustics of V1 at design flow rate and the “suction-side” winglet for high volume flow rates. However, as stated before, the direct comparison between the winglet variations and the “neutral” winglet is more appropriate. Therefore, for the one-third-octave band figures, V1 is removed from the analysis.

The results of the one-third-octave band analysis are shown in Figure 4. In overload ($\varphi = 0.27$ in Figure 4 (b)), all curves show a similar trend for the first and second harmonics. In the broadband frequency range between 400 and 1500 Hz, the curves have differences. The “pressure-side” winglet has the lowest sound power level, followed by the “suction-side” winglet. This trend can also be seen at the design point ($\varphi = 0.23$ in Figure 4 (c)) for the “pressure-side” winglet. The “suction-side” winglet deteriorates the noise emission in the broadband range at further throttled operating points. This observation corresponds to the sound power sum results as the “suction-side” winglet loses the acoustic advantage faster. Yet, a reduction in tonal frequencies can be seen for all winglet configurations at the design point. The “pressure-side” winglet has the lowest maximum peak, at about 68 dB. In comparison, the first harmonic of the “neutral” variant has a value of over 70 dB. Thus, there seems to be an influence potential for the tonal versus the broadband noise component by the winglet design. Optimization of the winglet geometry may reduce the tonal components even further. In partial-load ($\varphi = 0.21$ in Figure 4 (d)), the overall noise emission of all configurations (“pressure-“and “suction-side”) is significantly increased compared to the “neutral” winglet. Only the “pressure-side” winglet can compete with the “neutral” winglet in broadband frequencies. Again this fits the sound power level measurements well.

Further investigations are carried out for the “pressure-side” and “suction-side” winglets in order to get a better understanding of the mechanisms leading to the advantages.

Wall pressure measurements

In Figure 5, the results of wall pressure measurements are shown. Blue areas indicate an area of low pressure on the suction side of the blade, while red areas indicate a slight over-pressure. Notice that the scale is shifted asymmetrically, to indicate $c_p = 0$ as white areas. The rotating blade can be identified by the sharp-edged transition between areas of high and low pressure. The tip vortex can be identified as a bluish area above the blade. The main flow direction is from left to right.

Figure 5 (a-c) shows the comparison of c_p-distributions of different winglet variants at the design point. The tip vortices of the “pressure-side” and the “suction-side” winglet are more stable, stronger, and dissipate later. The tip vortices of the “pressure-side” winglet are the most stable (relative to the circumferential position). The turbulence of a decaying vortex may induce as broadband noise. Therefore, the more stable vortex may be the reason for the better broadband noise results of the winglets at the design point (see Figure 4 bottom left).

Further, the pressure difference across the tip gap is considered. The “neutral” winglet shows the highest pressure difference. The “pressure-side” winglet shows a lower pressure rise on the blade's pressure side (light red area) while the pressure drop on the suction side of the “suction-side” winglet (light blue area) is reduced. The vortex region of “pressure-“ and “suction-“ side winglets is shifted away from the blade. Thus, the vortex regions are bigger compared to the “neutral” winglet. The shift is confirmed by additional measurements of high-resolution pressure probes that have been embedded in the pressure and suction side surface of a blade. With installed winglets the pressure amplitude on the suction side of the blade decreases. Presumably the geometry of the winglet causes the shift of the position of the vortex. The distance between the blade and the axis of

the vortex increases. The greater distance reduces the interaction of the vortex with the blade itself, which reduces the sound power level. Even the “pressure-side” winglet can influence the position of the vortex on the suction side. Therefore, the interaction of the forming tip gap vortex with the vortex-generating blade has a more notable effect on the acoustics than the interaction of the impacting vortex on the subsequential blade.

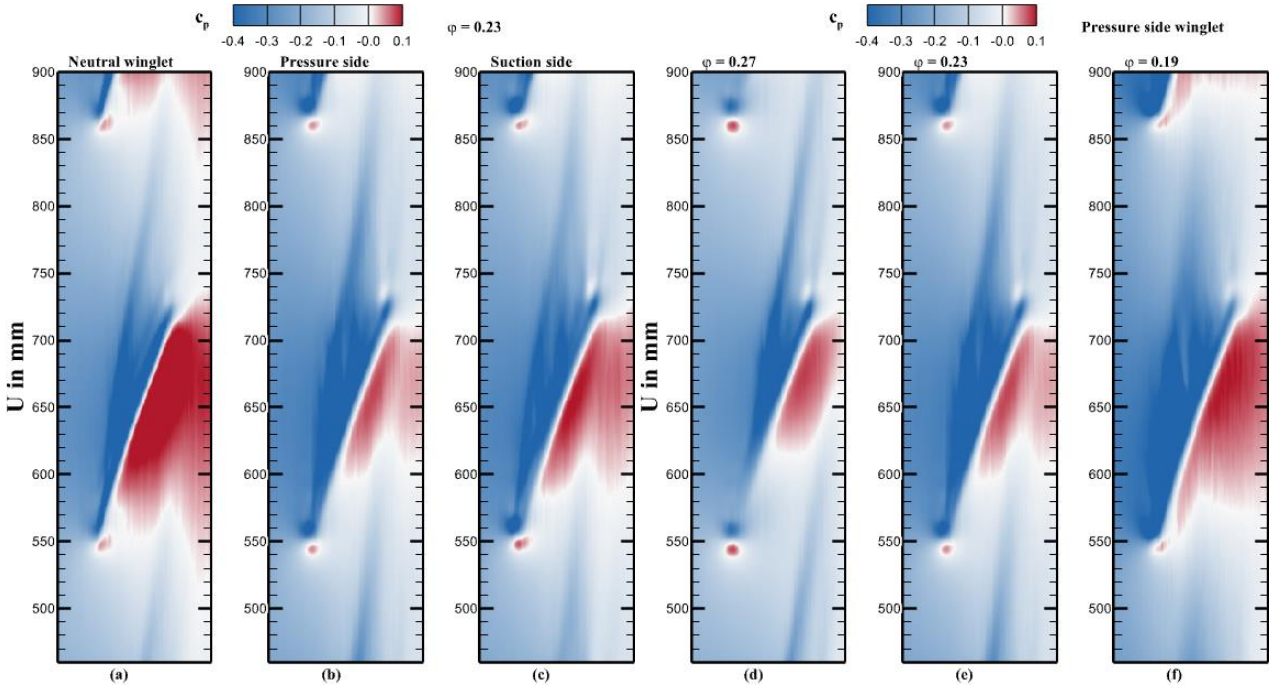

Figure 5: Wall pressure comparison at design point (a-c); processing of wall pressure of “pressure-side” winglet (d-f)

The “pressure-side” winglet is the most interesting regarding its acoustic effects. Therefore, three different operating points are shown for the “pressure-side” winglet in Figure 5 (d-f). For high φ = 0.27 (d), the tip vortex starts at about 20 percent chord length. The vortex boundary is distinct, and the vortex trajectory does not hit the neighbor blade in any of the configurations investigated. At the design point (e), the vortex trajectory is straightened up compared to the overload (d). The beginning of the vortex shifts to the leading edge, while the vortex of the “neutral” winglet still starts at about 20 percent chord length (a). The trajectory is not affected thereby.

In partial load (f), the trajectory moves away from the blade even further, the vortex bursts, and loses its shape. The boundary of the vortex area is no longer visible. The vortex dissipates before it can reach the neighbor blade. The burst vortex increases the turbulence in the flow field. The increased turbulence leads to increased broadband noise. Comparing “neutral” and “pressure-side” winglets, the vortex of the “neutral” winglet in partial load, is much more stable and distinct. The pressure rise over the blade rises with decreasing flow coefficient, corresponding to the characteristic curve shown in Figure 1.

Additional Particle-Image-Velocimetry studies confirm the wall-pressure measurements regarding the dissipation and trajectory of the tip gap vortex. Since they give no additional insights, they are not further discussed in this paper.

SUMMARY AND CONCLUSION

This paper aims to investigate the influence of generic winglets on the tip gap vortex of low speed axial fans. Therefore, three different winglet designs have been investigated. The results are compared to a baseline fan (V1) and a "neutral" winglet configuration.

A qualitative connection between the local design of the blade tip and the effects on the tip gap vortex on the one hand and the acoustics, on the other hand, has been shown. A 3D design (winglet or local dihedral) essentially leads to a less distinct vortex area. The difference in the vortex shape leads to a reduction of tonal and broadband components in overload. At partial load, the positive effect on the broadband noise is reduced so that both effects compensate each other up to overcompensation.

At overload up to the design point, a reduction of the sound power level for the “suction-side” and “pressure-side” winglet has been shown. In the one-third octave spectrum, the reduction is essentially coupled to tonal components. This improvement has a rather broadband character at partial load. For both configurations, the tip gap vortex does not interact visibly with the pressure side of the neighbor blade. Thus it is deduced that the interaction of the vortex with the blade suction side is the more significant noise source. The comparison of the upstream and downstream sound power levels confirms this conclusion. The design of the blade tip influences the strength of the tip vortex and its interaction with the blade.

The winglets have a measurable impact on the fan, although their geometrical size. They reduce the aerodynamic performance but can reduce noise. Thus further investigations of the tip gap design and the tip vortex have the potential of further improvement of low-pressure axial fans. If the design of the winglet is further improved, the aerodynamic disadvantages may even become negligible.

ACKNOWLEDGEMENTS

The authors would like to thank the research association Forschungsvereinigung für Luft- und Trocknungstechnik (FLT) e.V. for financial support of the research project AiF-Nr.: 18836 N/1. This project was carried out under the auspices of the Federation of Industrial Research Associations (AIF) and financed within the budget of the Federal Ministry of Economics and Technology Germany (BMWi).

NOMENCLATURE

A,B	Form parameters	u	Rotational speed
c_p	Pressure Coefficient	U	Circumferential position
D	Diameter	q_V	Volume flow rate
$L_w(A)$	Sound power level (A-weighted)	x	Axial coordinate
l	Chord length	Δ	Difference
n	Rotational speed	δ	Arc angle
p	Pressure	η	Efficiency
P	Power	ν	Hub to tip ratio
R	Nondimensional radius	ρ	Density
Re	Reynolds number	φ	Flow coefficient
s	Tip clearance	ψ	Pressure rise coefficient

Subscripts

c	Casing	ps	Pressure side
h	Hub	t	Tip
mech	Mechanical	ts	Total-to-static

BIBLIOGRAPHY

[1] DIRECTIVE 2009/125/EC – *Establishing a framework for the setting of ecodesign requirements for energy-related products*, 21. Oct **2009**

[2] T. Carolus, M. Beiler – *Skewed Blades in Low Pressure Fans: A Survey of Noise Reduction Mechanism*, AIAA-97-1591 **1997**

[3] F. Kameier – *Experimentelle Untersuchung zur Entstehung und Minderung des Blattspitzen-Wirbellärms axialer Strömungsmaschinen*, Dissertation, Berlin, DLR, **1993**

[4] H. Marcinowski – *Einfluß des Laufradspaltes und der Luftführung bei einem Külhlgebläse axialer Bauart*, Motortechnische Zeitschrift (MTZ), No. 13, pp 259-262, **1953**

[5] M. Khorrami, F. Li, M. Choudhari – *Model Approach for Reducing Rotor Tip-Clearance-Induced Noise in Turbofan Engines*, AIAA Journal, Vol. 40(8), S. 1518-1528, **2002**

[6] T. Fukano, C.-M. Jang – *Tip Clearance Noise of Axial Flow Fans Operating at Design and Off-Design Condition*, Journal of Sound and Vibration, Vol. 275, S. 1027-1050, **2004**

[7] R. E. Longhouse – *Control of tip-vortex noise of axial flow fans by rotating shrouds*, Journal of Sound and Vibration Vol. 85(2), pp. 201-214, **1978**

[8] F. Kameier, T. Nawrot, W. Neise – *Experimental Investigation of Tip Clearance Noise in Axial Flow Machines*, Proceedings of 14th DGLR/AIAA Aeroacoustics Conference Aachen 1992, Bonn, Germany (92-02-040), **1992**

[9] L. Zhang, Y. Jin, Y. Jin – *Effect of Tip Flange on Tip Leakage Flow of Small Axial Flow Fans*, Journal of Thermal Science Vol. 23, No. 1, pp. 45-52, **2014**

[10] A. Corsini, F. Rispoli, A. G. Sheard – *Shaping of Tip End-Plate to Control Leakage Vortex Swirl in Axial Flow Fans*, Journal of Turbomachinery Vol. 132(3):031005, **2010**

[11] A. Nashimoto, N. Fujisawa, T. Akuto, Y. Nagase – *Measurements of Aerodynamic Noise and Wake Flow Field in a Cooling Fan with Winglets*, Journal of Visualization Vol. 7, No. 1, pp. 85-92, **2004**

[12] C. Zhang, L. Ji, L. Zhou, S. Sun – *Effect of blended blade tip and winglet on aerodynamic and aeroacoustic performances of a diagonal fan,* Aerospace Science and Technology, Vol. 98, **2020**

[13] DIN EN ISO 5801:2008 – *Industrieventilatoren - Leistungsmessung auf genormten Pruefstaenden*, Oct. **2008**

[14] DIN EN ISO 5167-3:2003 – *Durchflussmessung von Fluiden mit Drosselgeräten in voll durchströmten Leitungen mit Kreisquerschnitt - Teil 3: Duesen und Venturiduesen*, Jan. **2003**

[15] T. Lindemann, J. Friedrichs, U. Stark – *Development of a New Design Method for High Efficiency Swept Low Pressure Axial Fans with Small Hub Ratio*, Proceedings of ASME Turbo Expo 2014: Turbine Technical Conference and Exposition 2014, Duesseldorf, Germany (GT2014-25932), **2014**

[16] H. Schlichting, E. Truckenbrodt - *Aerodynamik des Flugzeuges (Band 2) - Aerodynamik des Tragfluegels, des Rumpfes, der Fluegel-Rumpf-Anordnung und der Leitwerke*, 2. Ed. Springer-Verlag, Berlin, Germany, **1969**

[17] A. Skorpel, P. Frantzheld, J. Friedrichs - *Influence of blade sweep on aerodynamics and acoustics of low-pressure axial fans*, Proceedings of FAN 2018, Darmstadt, Germany, **2018**

[18] F. Mode - *Ventilatorenanlagen - Theorie, Berechnung, Anwendung*, 4th ed. deGruyter-Verlag, Berlin, Germany, **1972**

[19] B. Eck – *Ventilatoren - Entwurf und Betrieb der Radial-, Axial und Querstromventilatoren*, 6th ed. Springer-Verlag, Berlin, Germany, **2003**

[20] ZIEHL-ABEGG SE – *Tested Innovation*, Retrieved November 30, 2021 from https://www.ziehl-abegg.com/service/downloads?tx_hbziehlabegg_downloads%5Baction%5D=download&tx_hbziehlabegg_downloads%5Bcontroller%5D=Download&tx_hbziehlabegg_downloads%5Bfile%5D=10916&cHash=28c8e7fcdf75f0ff352d52978f68ac76, **2021**

[21] DIN EN ISO 3745:2012 + Amd 1:2017 – *Bestimmung der Schallleistungs- und Schallenergiepegel von Geräuschquellen aus Schalldruckmessungen - Verfahren der Genauigkeitsklasse 1 für reflexionsarme Räume und Halbräume*, Oct. **2017**

[22] S. Karstadt, M. Hess, B. Matyschok, P. F. Pelz – *The Influence of Tip Clearance on the Acoustic and Aerodynamic Characteristics of Fans*, Proceedings of ASME Turbo Expo 2010: Power for Land, Sea and Air, Glasgow, UK (GT2010-22082), **2010**